HHS Public Access

Author manuscript

Mol Cancer Res. Author manuscript; available in PMC 2017 March 01.

Published in final edited form as:

Mol Cancer Res. 2016 March ; 14(3): 287–295. doi:10.1158/1541-7786.MCR-15-0307.

Cancer-associated Fibroblasts Induce a Collagen Cross-link Switch in Tumor Stroma

Daniela Pankova[1], **Yulong Chen**[1], **Masahiko Terajima**[2], **Mark J. Schliekelman**[3], **Brandi N. Baird**[1], **Monica Fahrenholtz**[4], **Li Sun**[1], **Bartley J. Gill**[4], **Tegy J. Vadakkan**[5], **Min P. Kim**[6], **Young-Ho Ahn**[7], **Jonathon D. Roybal**[1], **Xin Liu**[1], **Edwin Roger Parra Cuentas**[8], **Jaime Rodriguez**[8], **Ignacio I. Wistuba**[8], **Chad J. Creighton**[9,10], **Don L. Gibbons**[1], **John M. Hicks**[11], **Mary E. Dickinson**[5], **Jennifer L. West**[12], **K. Jane Grande-Allen**[4], **Samir M. Hanash**[13], **Mitsuo Yamauchi**[2,14], and **Jonathan M. Kurie**[1,14]

[1]Department of Thoracic/Head and Neck Medical Oncology, University of Texas MD Anderson Cancer Center, Houston, TX

[2]NC Oral Health Institute, University of North Carolina at Chapel Hill, Chapel Hill, NC

[3]Division of Public Health Sciences, Fred Hutchinson Cancer Research Center, Seattle, WA

[4]Department of Bioengineering, Rice University, Houston, TX

[5]Department of Molecular Physiology and Biophysics, Baylor College of Medicine, Houston, TX

[6]Department of Surgery, The Methodist Hospital Research Institute, Houston, TX

[7]Department of Molecular Medicine, Ewha Womans University School of Medicine, Seoul, Korea

[8]Department of Translational Molecular Pathology, University of Texas MD Anderson Cancer Center, Houston, TX

[9]Department of Medicine and Dan L. Duncan Cancer Center, Baylor College of Medicine, Houston, TX

[10]Department of Bioinformatics and Computational Biology, University of Texas MD Anderson Cancer Center, Houston, TX

[11]Department of Pathology, Texas Children's Hospital, Houston, TX

[12]Department of Biomedical Engineering, Duke University, Durham, NC

[13]Department of Clinical Cancer Prevention, University of Texas MD Anderson Cancer Center, Houston, TX

Abstract

Intratumoral collagen cross-links heighten stromal stiffness and stimulate tumor cell invasion, but it is unclear how collagen cross-linking is regulated in epithelial tumors. To address this question,

[14]Corresponding Authors: Jonathan M. Kurie, Department of Thoracic/Head and Neck Medical Oncology, Unit 432, MD Anderson Cancer Center, 1515 Holcombe Blvd., Houston, TX 77030. Phone: 713-745-6747; FAX: 713-792-1220; jkurie@mdanderson.org; or Mitsuo Yamauchi, North Carolina Oral Health Institute, School of Dentistry, University of North Carolina at Chapel Hill, NC 27599, USA, 919-537-3217 (phone), Mitsuo_yamauchi@unc.edu.

The authors have no conflicts of interest to disclose.

we used $Kras^{LA1}$ mice, which develop lung adenocarcinomas from somatic activation of a $Kras^{G12D}$ allele. The lung tumors in $Kras^{LA1}$ mice were highly fibrotic and contained cancer-associated fibroblasts (CAFs) that produced collagen and generated stiffness in collagen gels. In xenograft tumors generated by injection of wild-type mice with lung adenocarcinoma cells alone or in combination with CAFs, the total concentration of collagen cross-links was the same in tumors generated with or without CAFs, but co-injected tumors had higher hydroxylysine aldehyde-derived collagen cross-links (HLCCs) and lower lysine-aldehyde-derived collagen cross-links (LCCs). Therefore, we postulated that an LCC-to-HLCC switch induced by CAFs promotes the migratory and invasive properties of lung adenocarcinoma cells. To test this hypothesis, we created co-culture models in which CAFs are positioned interstitially or peripherally in tumor cell aggregates, mimicking distinct spatial orientations of CAFs in human lung cancer. In both contexts, CAFs enhanced the invasive properties of tumor cells in 3-dimensional (3D) collagen gels. Tumor cell aggregates that attached to CAF networks on a Matrigel surface dissociated and migrated on the networks. Lysyl hydroxylase 2 (PLOD2/LH2), which drives HLCC formation, was expressed in CAFs, and LH2 depletion abrogated the ability of CAFs to promote tumor cell invasion and migration.

Keywords

Lung cancer; cancer-associated fibroblasts; collagen; invasion

Introduction

Cancer-associated fibroblasts (CAFs) are a morphologically and functionally heterogeneous group of mesenchymal cells with diverse origins and play critical roles in the regulation of tumor fibrosis, immunosuppression, angiogenesis, and metastasis (1). CAFs exhibit migratory and contractile properties of myofibroblasts and secrete collagen, cytokines, and chemokines into tumor stroma (1). In experimental tumor models, CAFs function as ‘leader cells’ for sheets or groups of invading tumor cells by displaying unique behaviors to maintain the group’s organization and directionality. Positioned at the forefront, CAFs lead collectively migrating tumor cells by realigning impeding collagen fibers through proteolytic and force-mediated matrix remodeling, creating tracks through which invading tumor cells can move; these tracks remain patent after decellularization (2), implying that the realigned collagen fibers within the track walls have acquired a certain degree of stability through collagen cross-linking. However, it is unclear whether CAFs regulate collagen cross-linking.

Cross-link formation is preceded by a series of modifications of telopeptidyl and helical lysine (Lys) residues on collagen that determine the fate and biophysical properties of cross-links (3). For instance, specific Lys residues on procollagen α chains undergo hydroxylation in cells by lysyl hydroxylases (LH1, LH2, and LH3) encoded by distinct procollagen-lysine, 2-oxoglutarate 5-dioxygenase (*PLOD*) genes (4–9). Lys and hydroxylysine (Hyl) residues in both N- and C-terminal telopeptides are then oxidatively deaminated into aldehydes (Lys^{ald} and Hyl^{ald}, respectively) by lysyl oxidase (LOX) in the extracellular space (10). Hyl^{ald} forms aldimine cross-links that spontaneously rearrange into stable ketoamines, which

further mature into stable Hyl^{ald}–derived trivalent cross-links (HLCCs) (10). In contrast, Lys^{ald} residues form a labile aldimine or an aldol condensation product that further matures into less stable Lys^{ald}–derived collagen cross-links (LCCs) (10). Implicating a potential role for HLCCs in tumor progression, high LH2 levels predict a poor prognosis in epithelial and other tumor types, and ectopic LH2 expression in tumor cells induces a LCC-to-HLCC switch in tumor stroma and stimulates tumor cell migration, invasion, and metastasis (11–14).

To gain insight into how collagen cross-linking is regulated during epithelial tumorigenesis, we used $Kras^{LA1}$ mice, which develop lung adenocarcinomas from somatic activation of a latent *K-ras*^{G12D} allele (15). Lung tumors in $Kras^{LA1}$ mice contain a population of CAFs that express Thy-1 (CD90), which marks a subset of lung fibroblasts in humans and mice (16–19), have myofibroblastic properties, and secrete diverse regulators of angiogenesis and inflammation (16).

Materials and Methods

Animal husbandry and syngeneic tumor cell injections

Before their initiation, all mouse experiments were submitted to and approved by the Institutional Animal Care and Use Committee at the University of Texas MD Anderson Cancer Center. $Kras^{LA1/+}$ mice and wild-type littermates received standards of care and were euthanized according to the standards set forth by the IACUC. As described previously (20), wild-type immunocompetent mice (n=10 per cohort, 30 total mice) were injected in the flank with 10^6 344SQ cells alone or co-injected with 5×10^5 344SQ cells and 5×10^5 CAFs. Cells and mice had syngeneic genetic backgrounds. Mice were necropsied 3 weeks after injection to measure weights of primary subcutaneous tumors and count the numbers of metastases on the lung pleural surfaces.

Isolation of CAFs

As described previously (16), murine CAFs were isolated from lung tissues at necropsy by immediately perfusing tissues with 2% fetal bovine serum in Hank's buffered salt solution (FBS-HBSS) and dispersing them into single cell suspension by immersion in 3 mg/mL of collagenase and Dispase®II (Roche) on a gentleMACS™ Dissociator (Miltenyi Biotec, Bergisch Gladbach, Germany) using the lung tissue dissociation programs (Lung_01 and Lung_02). Dispersed cells were centrifuged, washed with FBS-HBSS, and subjected to red blood cell lysis by adding RBC Buffer (BioLegend). The remaining cells were centrifuged, washed, filtered (70 μm and 40 μm), counted (Countess™, Invitrogen), and mixed twice with antibody-conjugated magnetic beads (Dynal-Magnetic beads, Invitrogen) on a rotator, each time for 45 min at 4°C, to first deplete leukocytes (anti-CD45 and anti-CD68, Abcam), endothelial cells (anti-CD31, BD Pharmingen), and epithelial cells (anti-EPCAM, Pharmingen) and then to isolate fibroblasts (anti-Thy-1, BD Pharmingen) from the supernatants. Fibroblasts were eluted off the anti-Thy-1-conjugated beads by incubation in FBS-HBSS, 0.5% BSA, and 2mM EDTA, centrifuged, washed, and cultured in RPMI1640 containing 10% FBS and 100 mg/100U penicillin-streptomycin (GIBCO).

Cell culture

CAFs were cultured in a-modified essential medium (MEM) (Cellgro) supplemented with 20% fetal bovine serum, penicillin/streptomycin, L-glutamine, and sodium pyruvate. Primary cells used in experiments had been passaged fewer than 6 times and were not tested for identity. The 344SQ cell line was cultured at 37°C and 5% CO_2 humidified atmosphere in RPMI 1640 (Mediatech) supplemented with 10% fetal bovine serum (Sigma), penicillin (100 U/ml) and streptomycin (100 μg/ml) (Sigma). Cells were treated with 20 μM GM6001 (EMD Millipore), 100 nM latrunculin (Sigma), or 25 μM blebbistatin (Sigma). 344SQ identity was confirmed by PCR analysis of known somatic mutations three month prior to performing experiments.

Creation of lung scaffolds

Lungs from adult $Kras^{LA1}$ mice were de-cellularized using methods previously described (21). In brief, lung tissue was harvested and native cells were removed using 1% sodium dodecyl sulfate and 1% Triton X-100 diluted in H_2O in a de-cellularization chamber.

Transmission electron microscopy

Transmission electron microscopy was performed on glutaraldehyde-fixed, plastic embedded subcutaneous tumor tissue or lung scaffolds as described previously (22).

Stiffness measurement

Cell-containing collagen gels and cell-free gels were mechanically tested by micropipette aspiration, as described previously (23). Briefly, glass micropipettes with an internal diameter of 90–110 μm were positioned at the surface of the samples. Vacuum pressure was applied by adjusting the height of a reservoir to aspirate the sample. At each pressure step, the reservoir height was recorded and an image was captured with an AxioCam MRm camera (Zeiss), which was later analyzed using ImageJ software (NIH) to measure the aspiration length and pipette diameter. Data analysis was performed via a MATLAB code to find the linear portion of the stress-strain curve and fit a line to this portion of the data by linear regression. To calculate the Young's modulus from the slope of the linear region, a half-space punch model was applied, assuming a value of 2.2 for the wall function (23).

Collagen cross-link analysis

Tissues were pulverized in liquid nitrogen using a Spex Freezer Mill (Spex, Inc.), washed with cold phosphate-buffered saline and cold distilled water, lyophilized and weighed. Aliquots were reduced with standardized NaB^3H_4 and hydrolyzed with 6N HCl. The hydrolysates were then subjected to amino acid and cross-link analyses (11, 24). The collagen content was determined as hydroxyproline/total amino acids based on the value of 100 residues of hydroxyproline per 1,000 amino acids in collagen. The reducible cross-links, dehydro [deH]-hydroxylysinonorleucine and its ketoamine (HLNL), deH-dihydroxylysinonorleucine and its ketoamine (DHLNL), and dehydro-histidinohydroxymerodesmosine (HHMD) were identified and measured as their reduced forms. The mature trivalent cross-links, pyridinoline (Pyr) and deoxypyridinoline (d-Pyr), were simultaneously analyzed by their fluorescence. All cross-links were quantified as

mol/mol of collagen based on the value of 300 residues of hydroxyproline per collagen molecule.

Generation of shRNA transfectants

We used shRNAs against human LH2 (SHC [V2LHS_131378] and SHD [V3LHS_306074) in pGIPZ system (shRNA and ORFeome Core, MD Anderson Cancer Center). pGIPZ-FF2 control, which targets the Firefly luciferase gene, was a gift from Kenneth Scott (Baylor College of Medicine). Cells were infected with lentiviruses carrying target-specific or control shRNA packaged in 293T cell using pMD2.G, and psPAX2 plasmids for 48 hours then selected with puromycin (10 μg/ml) for two weeks.

Co-culture assays

Multicellular aggregates were generated by using the hanging-drop method (25). In brief, 344SQ cells were detached with 2 mM EDTA, re-suspended in MEM supplemented with methylcellulose (20%) (Sigma) and growth factor-reduced Matrigel (1%) (BD Biosciences), and incubated as droplets (25 μl) containing 1,000 cells for 48 h to ensure multicellular aggregation. To generate mixed cell aggregates, equal numbers of 344SQ cells and CAFs were mixed (1,000 cells per droplet).

For collagen invasion assays, aggregates were washed with medium, mixed with rat-tail collagen solution (Serva) (2.0 mg/ml) containing 120,000 CAFs, pipetted as a drop-matrix, polymerized at 37°C, and replaced with medium. Aggregate invasion was analyzed 24 hours after seeding. An aggregate was scored as invasive if it had 2 or more protrusions that were at least ½ as long as the diameter of the aggregate. At least 200 aggregates were counted per condition. For leader-follower type of migration, hybrid aggregates were plated on top of Matrigel and cultured for 6 days when CAF and tumor cell migration were apparent as projections from the aggregate. For interactions with CAF networks, tumor aggregates were washed and plated on top of Matrigel. Afterwards, CAFs were stained for 30 minutes with CellTracker™ (Molecular Probes, Invitrogen), and 40,000 CAFs were added as single cell suspensions on top of aggregates. Network formation and collective tumor cell migration were evident at 24 hours. Images were captured by using Olympus U-LH100HG with Olympus 10x/0.30 Ph1 objectives.

Time-lapse microscopy

CAFs seeded with tumor aggregates on matrigel were monitored at 37°C using a motorized inverted Nikon Ti microscope (10 ×/0.30 NA air and 20×/1.0 NA objective lens; Leica) connected to EMCCD camera for up to 24 h.

Immunofluorescence microscopy

Cells were seeded and grown on coverslips and fixed after 24 hours in 4% paraformaldehyde (Electron Microscopy Sciences, PA,USA) for 15 minutes at room temperature and then permeabilized with 0.5% Triton X-100 (Sigma) in PBS for 10 minutes at room temperature. Non-specific binding was blocked with 3% bovine serum albumin (Sigma) in PBS for 30 minutes before incubation with a primary antibody against type I collagen (Md Bioproducts) for 2 hours at room temperature. Secondary antibody was

incubated for 1 hour at room temperature, after which DAPI was incubated for 15 minutes, with extensive washing between each step. Images were captured by using Olympus U-LH100HG with Olympus 10×/0.30 Ph1 or 4×/0.10 objectives.

Second harmonic generation using two-photon microscopy

Second harmonic generation signal from collagen and the emission signal from 344SQ-RFP were detected upon simultaneous excitation with a 920 nm laser. The signal from collagen was collected using a BP 460/50 filter. The emission signal from RFP was collected using an LP 515 filter. The images were acquired using the LSM 7 MP microscope (Carl Zeiss, Jena, Germany) using the Zeiss W Plan-Apochromat 20×/1.0 NA objective lens.

Statistical analysis

All quantitative values represent the means of replicate samples and are representative of multiple experiments. Numerical values of cell culture and mouse cohort data were analyzed using student's t-test for significance in GraphPad software. The difference was considered significant at $P < 0.05$ (two-tailed). All computations were carried out in SAS 9.2 and S-plus 8.0.

Results

CAFs promote intratumoral fibrosis in $Kras^{LA1}$ mice

To determine whether lung tumors in $Kras^{LA1}$ mice are fibrotic, we decellularized whole lung tissues and inspected the stroma, which showed that tumor stroma was denser than that of adjacent normal lung and contained compact collagen bundles (Fig. 1A). In intact lung tissues, tumors contained abundant collagen surrounding tumor cells and fibroblastic cells (Fig. 1B, C). To determine whether CAFs regulate intratumoral fibrosis, we isolated Thy-1+ CAFs from $Kras^{LA1}$ mice and examined their ability to produce collagen and to align collagen fibers and generate stiffness in collagen gels. In monolayer culture, CAFs secreted collagen into extracellular space (Fig. 1D). To determine whether CAFs regulate collagen fiber alignment, we performed second harmonic generation (SHG) analysis on collagen gels seeded with CAFs and 344SQ cells, a highly invasive and metastatic lung adenocarcinoma cell line derived from mice that co-express $Kras^{LA1}$ and $p53^{R172H}$ alleles (20). Although minimal SHG signal was detected in gels seeded with 344SQ cells alone, those seeded with 344SQ cells and CAFs produced an intense signal (Fig. 1E). The CAFs contracted and organized the collagen gel, generating an elastic modulus that was significantly greater than the collagen gel alone (Fig. 1F). Thus, lung tumors in $Kras^{LA1}$ mice were fibrotic and contained CAFs that produced collagen and exhibited collagen remodeling activity.

CAFs regulate the type of collagen cross-link in tumor stroma

To determine whether CAFs regulate collagen cross-linking in tumors, we subcutaneously injected 344SQ cells alone (10^6) or in combination with CAFs (5×10^5) into syngeneic, immunocompetent mice to generate flank tumors, which were analyzed for total collagen cross-links, HLCCs (DHLNL, Pyr, and d-Pyr), LCCs (HHMD), and HLNL, which can be classified as HLCC or LCC depending on whether cross-links form between telopeptidyl Hyl^{ald} and helical Lys or telopeptidyl Lys^{ald} and helical Hyl, respectively (3). Although total

collagen cross-links were not different between the two cohorts (Fig. 2A), tumors containing ectopic CAFs had lower levels of the LCC HHMD (Fig. 2B), higher levels of the HLCCs Pyr and DHLNL (Fig. 2C), and lower levels of HLNL (Fig. 2D). The HLCC-to-LCC ratio in tumors containing ectopic CAFs was higher than that of tumors generated by 344SQ cells alone (6.54 ± 4.12 *versus* 1.90 ± 1.07, respectively) (Fig. 2E), indicating that CAFs induced a LCC-to-HLCC switch in tumor stroma.

Models to study how tumor cells respond to CAFs in different spatial orientations

In human lung cancer, CAFs are present in the interstitium and around the periphery of the tumor, and it is unclear how CAFs in these locations regulate tumor cell behavior (26). To address this question, we created 3-dimensional co-culture models that mimic the interstitial and peripheral locations of CAFs. Mixed 1:1 in hanging drops, 344SQ cells and CAFs formed cellular aggregates with a relatively uniform distribution, which we used to represent an interstitial CAF pattern. Two days after seeding onto a Matrigel surface, there were protrusions of tumor cells that remained adherent to the aggregates, and CAFs were visible at the tips of the tumor cell protrusions and elsewhere on the Matrigel surface (Fig. 3). In comparison, aggregates containing 344SQ cells alone developed no protrusions (Fig. 3). We concluded that “interstitial” CAFs emerged from the aggregates and enhanced tumor cell motility, possibly by functioning as “leader cells” at the tips of tumor cell protrusions (2). To create a model that recapitulates the peripheral location of CAFs, we seeded 344SQ cells into hanging drops, forming aggregates of 344SQ cells, which were encapsulated into collagen gels that did or did not contain CAFs. After 24 hours, aggregates were scored for the presence or absence of invasive protrusions (Fig. 4A). In the absence of CAFs, 20% of the aggregates developed invasive protrusions, whereas 60% developed protrusions in collagen containing CAFs (Fig. 4B). Protrusion formation was sharply diminished by treatment with a protease inhibitor (GM6001) (Fig. 4A and 4B), indicating that the protrusions had proteolytic activity. We concluded that CAFs in a peripheral location enhance tumor cell invasive activity. Lastly, because human lung cancers are occasionally interspersed with band-like fibrotic structures containing CAFs (27), we asked whether structures formed by CAFs provide a favorable matrix for tumor cell attachment and migration. CAFs were seeded onto a Matrigel surface and allowed to spontaneously form network structures with contractile activity (Fig. 5A and Supplementary Movie 1). Treatment with latrunculin A or blebbistatin caused dispersal of the structures (Fig. 5B), supporting the conclusion that actomyosin contractility maintains the integrity of the structures. Seeded onto the Matrigel surface, aggregates of 344SQ cells attached to the networks, spontaneously dissociated, and migrated along the networks (Figs. 5C, D, and Supplementary Movie 2). Collectively, these findings show that CAFs in different spatial locations enhance the migratory and invasive activities of lung adenocarcinoma cells.

LH2 expression in CAFs promotes lung adenocarcinoma cell migration and invasion

While all 3 LH family members hydroxylate Lys residues in the helical sequence of collagen, LH2 is the only family member that is capable of hydroxylating telopeptidyl Lys residues and is indispensable for the formation of HLCCs (3). To determine whether the LCC-to-HLCC switch induced by CAFs influences the migratory and invasive behaviors of tumor cells, we generated two LH2-deficient CAF populations by stably transfecting distinct

LH2-specific short hairpin RNAs (shRNAs) (Fig. 6A). Relative to the control transfectants, the LH2-deficient CAFs generated less stiffness in collagen gels, although to different degrees (Fig. 6B). LH2 deficiency reduced the ability of CAFs to induce protrusion formation from the interstitium or periphery of tumor cell aggregates (Figs. 6C and 6D). Seeded on a Matrigel surface, LH2-deficient CAFs formed poorly defined networks that failed to promote the dissociation and migration of tumor cell aggregates (Fig. 6E).

Discussion

In squamous carcinomas with low cell-autonomous invasive activity, CAFs proteolytically degrade tumor stroma to create tracks through which tumor cells can collectively invade (2), which is the basis for the working hypothesis that CAFs compensate for deficiencies in tumor cell-autonomous invasive activity. Here we show that CAFs enhance the migration and invasion of tumor cells with high cell-autonomous invasive activity, implying that CAFs may exert pro-invasive activity in a broader tumor cell context than previously thought. By showing that CAFs regulate collagen cross-linking, the findings presented here build on evidence that CAFs induce proteolysis and force-mediated realignment of collagen fibers (2).

Pharmacologic and genetic approaches to inhibit LOX in tumors have shown that LOX is the primary driver of collagen cross-link formation and that the total amount of collagen cross-links is correlated with tumor stiffness (28). However, LH2 regulates tissue stiffness by determining the types, rather than the total amounts, of collagen cross-links. HLCCs are more stable than LCCs and are the primary type of cross-link in skeletal tissues like bone and cartilage, which require HLCCs to maintain tissue stiffness and integrity (3). Abnormally high HLCC levels are associated with arthritic conditions such as systemic sclerosis, whereas deficiencies are associated with severe soft-tissue and skeletal deformities such as those in patients with Bruck syndrome (29). Findings presented here add to a growing body of evidence that high HLCC levels contribute to the pathogenesis of cancer (11).

Using in vitro models that mimic epithelial tumor acini within a 3-dimensional matrix, here we showed that tumor cell aggregates respond to signals from CAFs. Of particular interest was the finding that CAFs formed contractile networks, tumor aggregates adherent to the networks disorganized and migrated, and depletion of LH2 expression in CAFs diminished network formation and tumor aggregate dissociation. Conversely, multicellular epithelial structures have been shown to exert contractile forces that mechanically reorganize collagen networks over long distances and in a highly directional manner, generating what are variously coined fibers, tracts, cables, straps, or lines (30–35). Moreover, regions of highly directional collagen alignment have been seen in tumor explants and clinical samples and are associated with poor clinical outcomes in patients with breast cancer (36). In conclusion, the model presented here may inform how epithelial tumor acini interact with surrounding stroma to generate mechanical and biochemical signals that regulate malignant tumor progression.

We did not observe a difference in the number of metastases in mice injected with or without CAFs, but both cohorts had high numbers of metastases, which reduces our ability to detect subtle differences. Moreover, a central finding from our co-culture assays is that tumor cells with autonomous metastatic activity can also migrate and invade in response to CAFs, potentially gaining the capacity to metastasize through non-autonomous mechanisms. Although its clinical relevance is unclear, this finding demonstrates the versatility of metastatic tumor cells and raises the possibility that therapeutic approaches to prevent metastasis may have to address both mechanisms.

Acknowledgments

This work was supported in part by R01CA157450 (JMK and MY), Cancer Prevention Research Institute of Texas Multi-investigator Research Award RP120713 (JMK, DLG, CJC), P50 CA70907 (JMK), P30 CA125123 (CJC), K08 CA151651 (DLG), and an MD Anderson Physician-Scientist Award (DLG). We thank Yiqun Zhang and Fengiu Chen for technical assistance.

References

1. Ohlund D, Elyada E, Tuveson D. Fibroblast heterogeneity in the cancer wound. J Exp Med. 2014; 211:1503–1523. [PubMed: 25071162]
2. Gaggioli C, Hooper S, Hidalgo-Carcedo C, Grosse R, Marshall JF, Harrington K, et al. Fibroblast-led collective invasion of carcinoma cells with differing roles for RhoGTPases in leading and following cells. Nat Cell Biol. 2007; 9:1392–1400. [PubMed: 18037882]
3. Yamauchi M, Sricholpech M. Lysine post-translational modifications of collagen. Essays Biochem. 2012; 52:113–133. [PubMed: 22708567]
4. Mercer DK, Nicol PF, Kimbembe C, Robins SP. Identification, expression, and tissue distribution of the three rat lysyl hydroxylase isoforms. Biochem Biophys Res Commun. 2003; 307:803–809. [PubMed: 12878181]
5. Pornprasertsuk S, Duarte WR, Mochida Y, Yamauchi M. Lysyl hydroxylase-2b directs collagen cross-linking pathways in MC3T3-E1 cells. J Bone Miner Res. 2004; 19:1349–1355. [PubMed: 15231023]
6. Pornprasertsuk S, Duarte WR, Mochida Y, Yamauchi M. Overexpression of lysyl hydroxylase-2b leads to defective collagen fibrillogenesis and matrix mineralization. J Bone Miner Res. 2005; 20:81–87. [PubMed: 15619673]
7. Takaluoma K, Lantto J, Myllyharju J. Lysyl hydroxylase 2 is a specific telopeptide hydroxylase, while all three isoenzymes hydroxylate collagenous sequences. Matrix Biol. 2007; 26:396–403. [PubMed: 17289364]
8. Uzawa K, Grzesik WJ, Nishiura T, Kuznetsov SA, Robey PG, Brenner DA, et al. Differential expression of human lysyl hydroxylase genes, lysine hydroxylation, and cross-linking of type I collagen during osteoblastic differentiation in vitro. J Bone Miner Res. 1999; 14:1272–1280. [PubMed: 10457259]
9. van der Slot AJ, Zuurmond AM, Bardoel AF, Wijmenga C, Pruijs HE, Sillence DO, et al. Identification of PLOD2 as telopeptide lysyl hydroxylase, an important enzyme in fibrosis. J Biol Chem. 2003; 278:40967–40972. [PubMed: 12881513]
10. Eyre DR, Paz MA, Gallop PM. Cross-linking in collagen and elastin. Annu Rev Biochem. 1984; 53:717–748. [PubMed: 6148038]
11. Chen Y, Terajima M, Yang Y, Sun L, Ahn YH, Pankova D, et al. Lysyl hydroxylase 2 induces a collagen cross-link switch in tumor stroma. J Clin Invest. 2015; 125:1147–1162. [PubMed: 25664850]
12. Eisinger-Mathason TS, Zhang M, Qiu Q, Skuli N, Nakazawa MS, Karakasheva T, et al. Hypoxia-dependent modification of collagen networks promotes sarcoma metastasis. Cancer Discov. 2013; 3:1190–1205. [PubMed: 23906982]

13. Gilkes DM, Bajpai S, Chaturvedi P, Wirtz D, Semenza GL. Hypoxia-inducible factor 1 (HIF-1) promotes extracellular matrix remodeling under hypoxic conditions by inducing P4HA1, P4HA2, and PLOD2 expression in fibroblasts. J Biol Chem. 2013; 288:10819–10829. [PubMed: 23423382]
14. Gilkes DM, Bajpai S, Wong CC, Chaturvedi P, Hubbi ME, Wirtz D, et al. Procollagen lysyl hydroxylase 2 is essential for hypoxia-induced breast cancer metastasis. Mol Cancer Res. 2013; 11:456–466. [PubMed: 23378577]
15. Johnson L, Mercer K, Greenbaum D, Bronson RT, Crowley D, Tuveson DA, et al. Somatic activation of the K-ras oncogene causes early onset lung cancer in mice. Nature. 2001; 410:1111–1116. [PubMed: 11323676]
16. Roybal JD, Zang Y, Ahn YH, Yang Y, Gibbons DL, Baird BN, et al. miR-200 Inhibits lung adenocarcinoma cell invasion and metastasis by targeting Flt1/VEGFR1. Mol Cancer Res. 2011; 9:25–35. [PubMed: 21115742]
17. Bradley JE, Ramirez G, Hagood JS. Roles and regulation of Thy-1, a context-dependent modulator of cell phenotype. Biofactors. 2009; 35:258–265. [PubMed: 19422052]
18. Nazareth MR, Broderick L, Simpson-Abelson MR, Kelleher RJ Jr, Yokota SJ, Bankert RB. Characterization of human lung tumor-associated fibroblasts and their ability to modulate the activation of tumor-associated T cells. J Immunol. 2007; 178:5552–5562. [PubMed: 17442937]
19. Sanders YY, Pardo A, Selman M, Nuovo GJ, Tollefsbol TO, Siegal GP, et al. Thy-1 promoter hypermethylation: a novel epigenetic pathogenic mechanism in pulmonary fibrosis. Am J Respir Cell Mol Biol. 2008; 39:610–618. [PubMed: 18556592]
20. Gibbons DL, Lin W, Creighton CJ, Rizvi ZH, Gregory PA, Goodall GJ, et al. Contextual extracellular cues promote tumor cell EMT and metastasis by regulating miR-200 family expression. Genes Dev. 2009; 23:2140–2151. [PubMed: 19759262]
21. Mishra DK, Thrall MJ, Baird BN, Ott HC, Blackmon SH, Kurie JM, et al. Human lung cancer cells grown on acellular rat lung matrix create perfusable tumor nodules. Ann Thorac Surg. 2012; 93:1075–1081. [PubMed: 22385822]
22. Rodriguez-Waitkus PM, Byrd R, Hicks J. Metachromatic leukodystrophy and its effects on the gallbladder: a case report. Ultrastruct Pathol. 2011; 35:271–276. [PubMed: 22085303]
23. Krishnamurthy VK, Guilak F, Narmoneva DA, Hinton RB. Regional structure-function relationships in mouse aortic valve tissue. J Biomech. 2011; 44:77–83. [PubMed: 20863504]
24. Yamauchi M, Shiiba M. Lysine hydroxylation and cross-linking of collagen. Methods Mol Biol. 2008; 446:95–108. [PubMed: 18373252]
25. Foty R. A simple hanging drop cell culture protocol for generation of 3D spheroids. J Vis Exp. 2011
26. Karagiannis GS, Poutahidis T, Erdman SE, Kirsch R, Riddell RH, Diamandis EP. Cancer-associated fibroblasts drive the progression of metastasis through both paracrine and mechanical pressure on cancer tissue. Mol Cancer Res. 2012; 10:1403–1418. [PubMed: 23024188]
27. Bobba RK, Holly JS, Loy T, Perry MC. Scar carcinoma of the lung: a historical perspective. Clin Lung Cancer. 2011; 12:148–154. [PubMed: 21663856]
28. Perryman L, Erler JT. Lysyl oxidase in cancer research. Future Oncol. 2014; 10:1709–1717. [PubMed: 25145437]
29. Byers PH, Pyott SM. Recessively inherited forms of osteogenesis imperfecta. Annu Rev Genet. 2012; 46:475–497. [PubMed: 23145505]
30. Shi Q, Ghosh RP, Engelke H, Rycroft CH, Cassereau L, Sethian JA, et al. Rapid disorganization of mechanically interacting systems of mammary acini. Proc Natl Acad Sci U S A. 2014; 111:658–663. [PubMed: 24379367]
31. Provenzano PP, Inman DR, Eliceiri KW, Trier SM, Keely PJ. Contact guidance mediated three-dimensional cell migration is regulated by Rho/ROCK-dependent matrix reorganization. Biophys J. 2008; 95:5374–5384. [PubMed: 18775961]
32. Guo CL, Ouyang M, Yu JY, Maslov J, Price A, Shen CY. Long-range mechanical force enables self-assembly of epithelial tubular patterns. Proc Natl Acad Sci U S A. 2012; 109:5576–5582. [PubMed: 22427356]

33. Vader D, Kabla A, Weitz D, Mahadevan L. Strain-induced alignment in collagen gels. PLoS One. 2009; 4:e5902. [PubMed: 19529768]

34. Sawhney RK, Howard J. Slow local movements of collagen fibers by fibroblasts drive the rapid global self-organization of collagen gels. J Cell Biol. 2002; 157:1083–1091. [PubMed: 12058022]

35. Dhimolea E, Maffini MV, Soto AM, Sonnenschein C. The role of collagen reorganization on mammary epithelial morphogenesis in a 3D culture model. Biomaterials. 2010; 31:3622–3630. [PubMed: 20149444]

36. Conklin MW, Eickhoff JC, Riching KM, Pehlke CA, Eliceiri KW, Provenzano PP, et al. Aligned collagen is a prognostic signature for survival in human breast carcinoma. Am J Pathol. 2011; 178:1221–1232. [PubMed: 21356373]

Implications

CAFs induce a collagen cross-link switch in tumor stroma to influence the invasive properties of tumor cells.

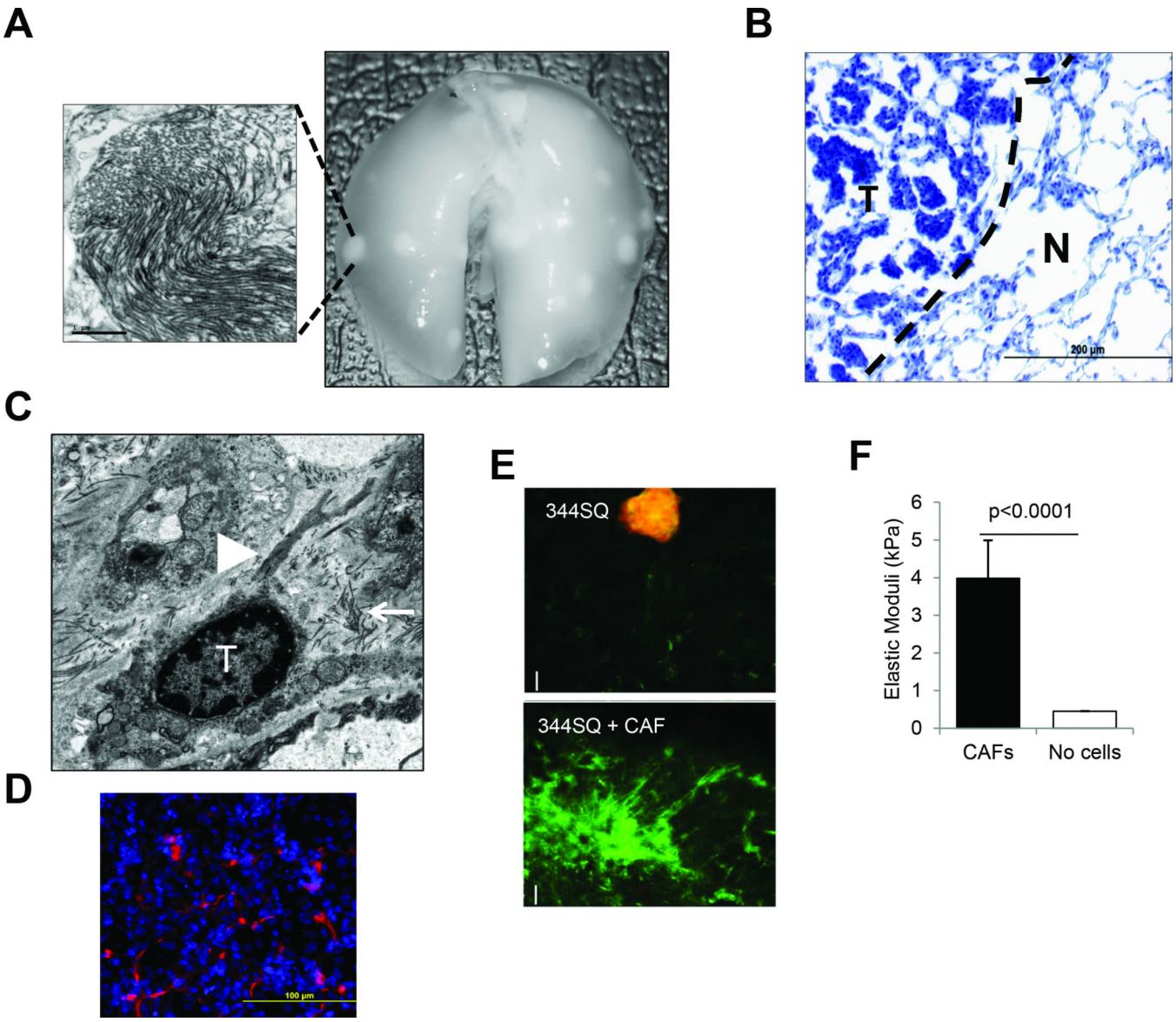

Figure 1.

Lung tumors in Kras^{LA1} mice are fibrotic. A, tissue scaffold created by detergent-based decellularization of lungs from a Kras^{LA1} mouse with areas of hyperdense stroma in tumoral regions that contain dense collagen bundles by transmission electron microscopic analysis (inset). Bar size, 1 μm. B, masson's trichrome staining (left panel) of collagen (blue) in lung tumor from a Kras^{LA1} mouse. Tumor (T). Normal lung (N). Bar size (200 μm). C, transmission electron microscopic analysis (right panel) of lung tumor from a Kras^{LA1} mouse. Tumor cell (T). Fibroblastic cell (arrowhead). Collagen bundles (arrow). D, immunocytochemical analysis of type I collagen (red) in CAFs grown in monolayer culture on plastic. Bar size, 100 μm. E, second harmonic generation images of 344SQ cells seeded alone or with CAFs into collagen gels. Collagen (green). Bar size, 200 μm. F, Young's modulus for cells entrapped in collagen gels. Gels containing CAFs (n=4) had significantly higher Young's modulus as compared to cell-free collagen gels (n=5), $p < 0.0001$.

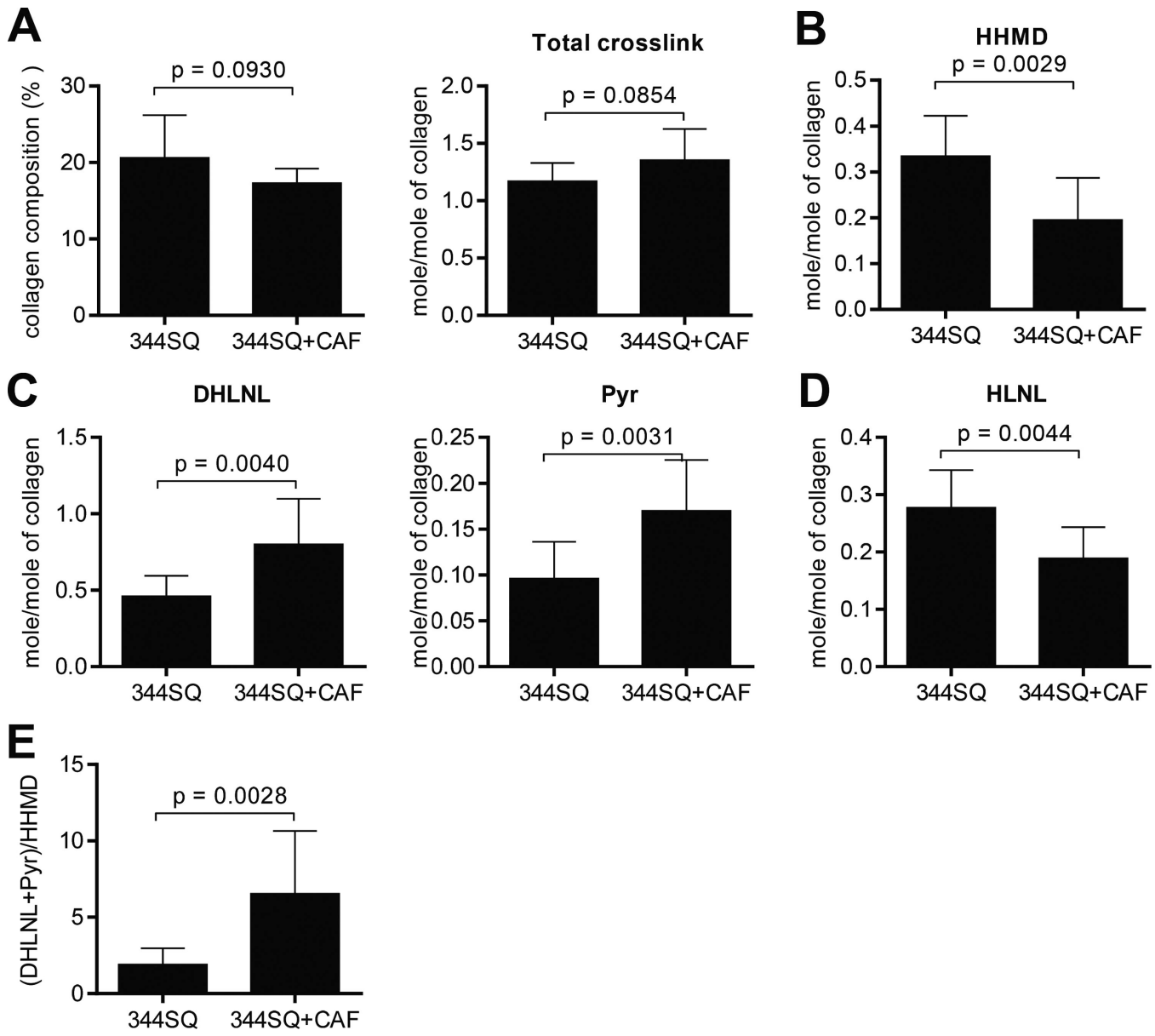

Figure 2.

Co-injection of CAFs induces a collagen cross-link switch in tumor stroma. A, quantification of collagen content (left bar graph) and total collagen cross-links (right bar graph) (mol/mol of collagen) in tumors generated by subcutaneous injection of 344SQ cells alone (344SQ) or in combination with CAFs (344SQ+CAF). B-D, tumors subjected to quantification of a LCC (HHMD) (B), HLCCs (DHLNL and Pyr) (C), and HLNL (D). Total cross-links in (A) were sum of cross-links in (B-D). E, HLCC-to-LCC ratio determined from (B) and (C).

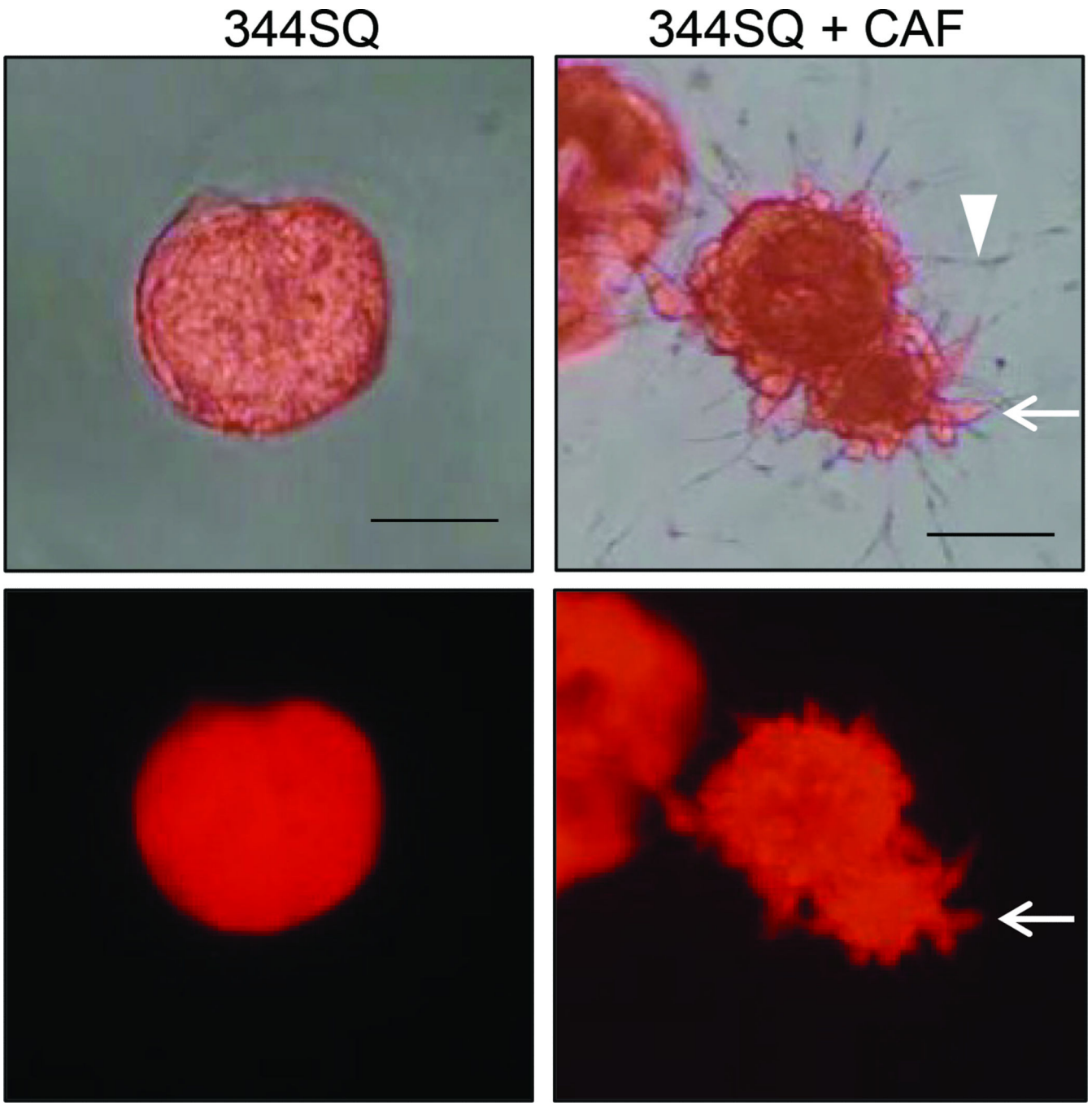

Figure 3.

Interstitial CAF model. Bright field (top) and fluorescence (bottom) micrographs of aggregates that contain RFP-tagged 344SQ cells alone (344SQ) or with untagged CAFs (344SQ + CAF) imaged 2 days after seeding. CAFs had emerged from the aggregates (arrowhead), and aggregates had developed projections of tumor cells (arrow). Bar size, 100 μm.

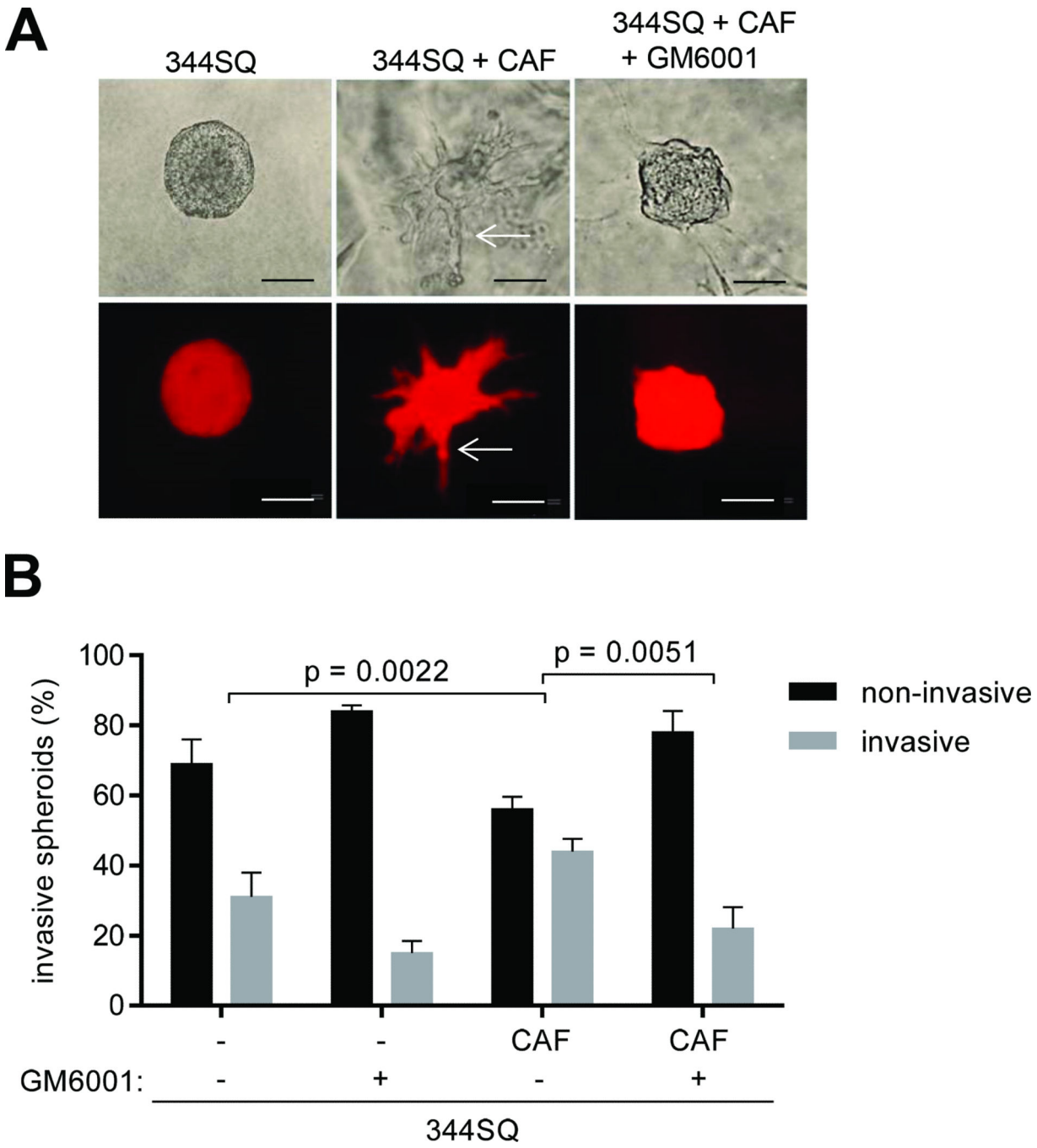

Figure 4.

Peripheral CAF model. A, bright field (top) and fluorescence (bottom) micrographs of aggregates that contain RFP-tagged 344SQ cells alone (344SQ) or with untagged CAFs (344SQ + CAF) in the presence or absence of GM6001. Projections of invasive tumor cells (arrows). Bar size, 100 μm. B, percentages of total aggregates (n=200 aggregates counted per condition) scored as invasive or non-invasive in the presence or absence of GM6001.

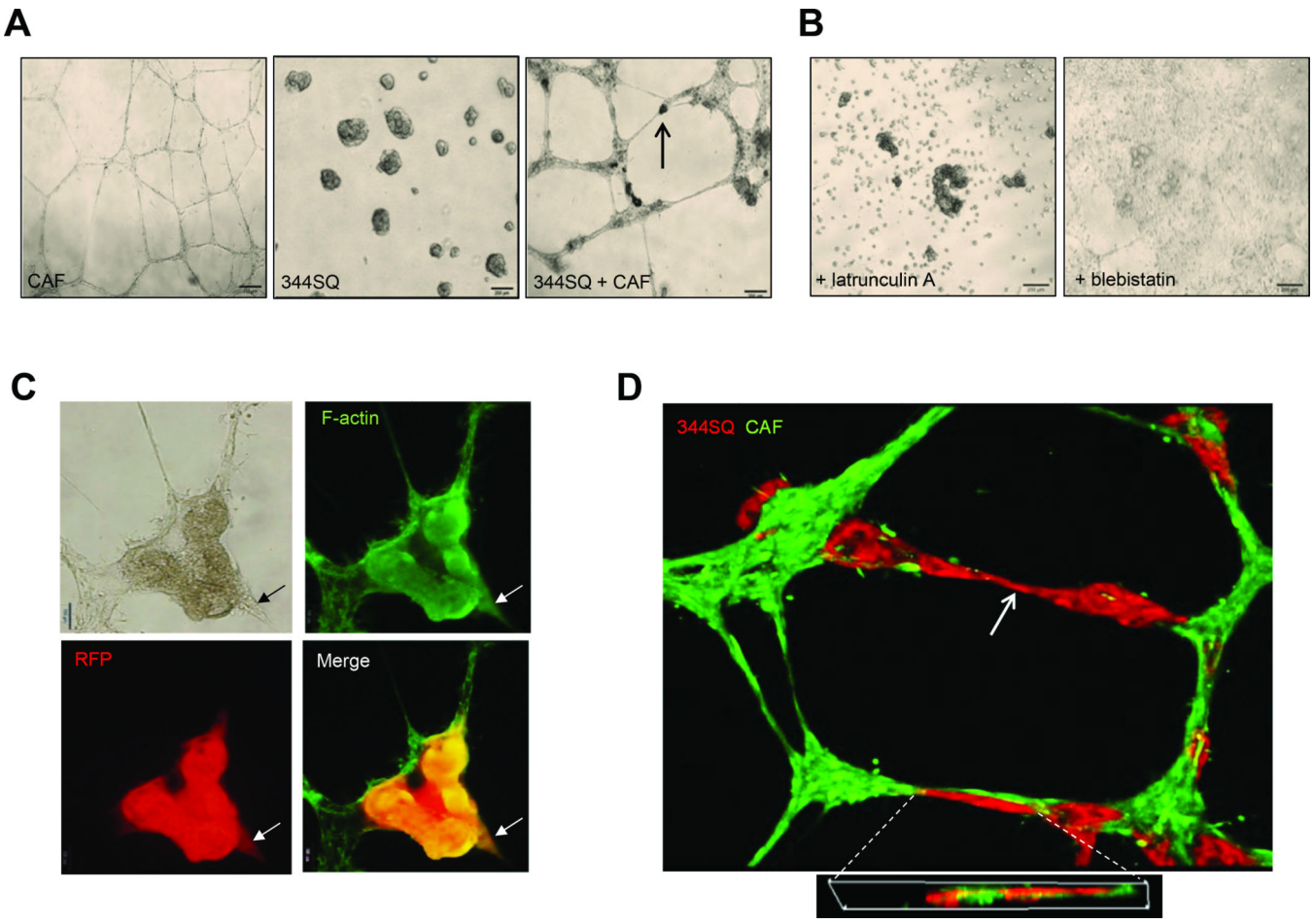

Figure 5.

Interaction of aggregates with CAF network structures. A, bright field micrographs of CAF structures alone (left panel), aggregates of 344SQ cells alone (middle panel), or 344SQ aggregates seeded on CAF structures (right panel). Bar size, 200 μm. B, bright field micrographs of 344SQ aggregates seeded on CAF structures in the presence of latrunculin A or blebbistatin. Bar size, 200 μm. C, bright field (top left panel) and fluorescence micrographs of a RFP-tagged tumor aggregate attached to CAF structures (green) imaged 2 days after seeding. Arrow points to region of aggregate that is beginning to dissociate and migrate along CAF networks. F-actin (green). Bar size, 20 μm. immunofluorescence microscopic images of RFP-tagged tumor cell aggregates containing 344SQ cells alone (344SQ) or hybrid aggregates containing 344SQ cells and LFs (344SQ + LF) or CAFs (344SQ + CAF) photographed 2 days after seeding on a Matrigel surface. E, F, immunofluorescence microscopic images of 2 RFP-expressing tumor aggregates (red) that have disorganized, migrated toward each other, and coalesced (arrow) on CAFs. CAFs pre-treated with cell tracker green. Photographed 2 days after seeding. Inset is Z-stack image of bracketed area. Bar size, 100 μm.

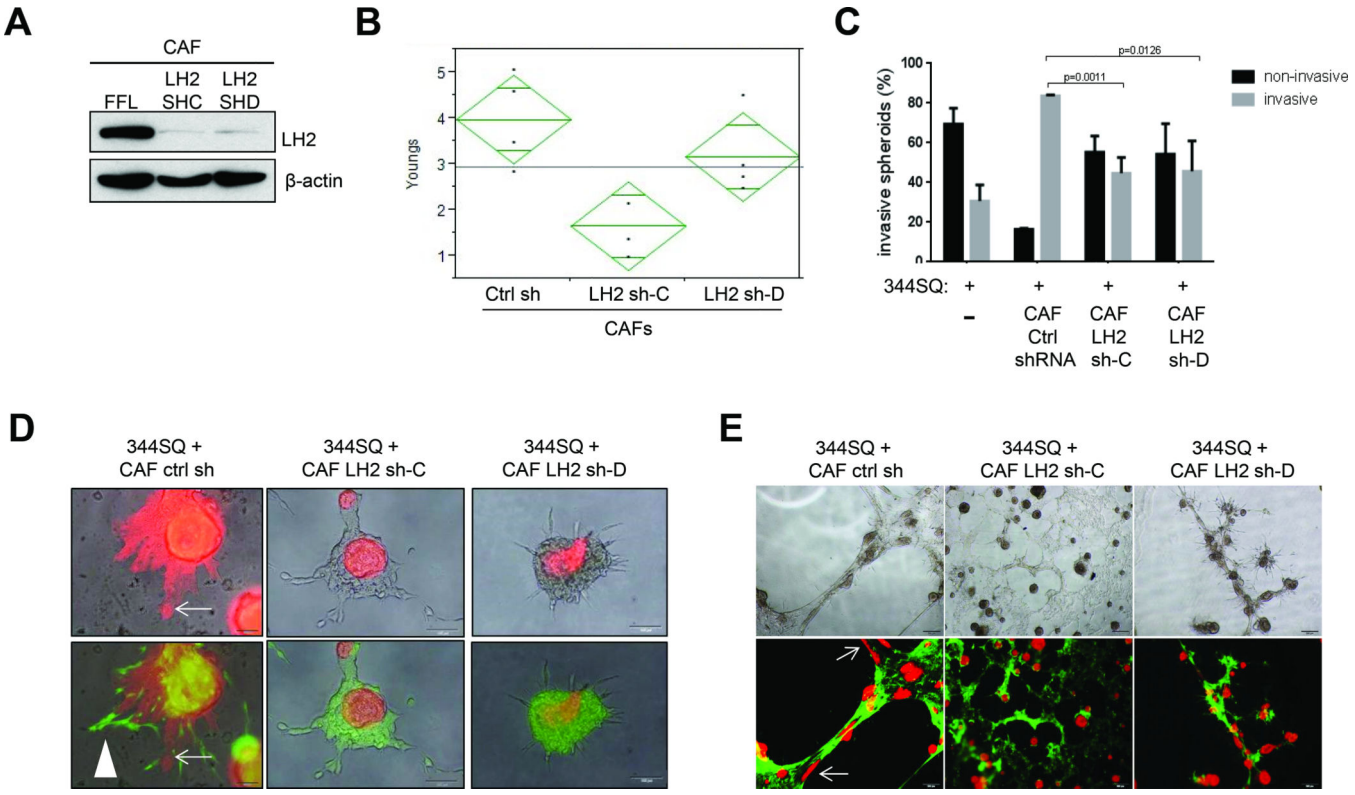

Figure 6.

LH2 is required for CAF-induced tumor aggregate migration and invasion. A, Western blot analysis of CAFs stably transfected with control (FFL) or LH2-specific (SHC, SHD) shRNAs. β-actin, loading control. B, Young's modulus for cells entrapped in collagen gels. SHC had a significantly lower Young's modulus as compared to control FFL) ($p < 0.01$) and tended to have a lower modulus than SHD, although not significant ($p = 0.0788$). C, percentages of total aggregates (n=200 aggregates counted per condition) scored as invasive or non-invasive in collagen gels containing no fibroblasts (−) or CAF transfectants. D, hybrid aggregates containing RFP-tagged tumor cells (344SQ) and GFP-tagged CAF transfectants and photographed under phase contrast (top panels) or fluorescence (bottom panels) microscopy 3 days after seeding on a Matrigel surface. Migratory tumor cells (arrow). Leading CAFs (arrowhead). Bar size, 100 μm. E, CAF transfectants and tumor aggregates (344SQ-RFP) were co-cultured on a Matrigel surface and photographed under phase contrast (top panels) and fluorescence (bottom panels) microscopy after 2 days. Dissociating tumor aggregates (arrows). Bar size, 200 μm.